Lateritic paleoweathering profiles in French Massif Central: Paleomagnetic datings

Caroline Ricordel-Prognon, France Lagroix, Marie-Gabrielle Moreau, Médard Thiry

Lateritic paleoweathering profiles in French Massif Central: Paleomagnetic datings

Caroline Ricordel-Prognon,[1,2] France Lagroix,[3] Marie-Gabrielle Moreau,[3] and Médard Thiry[1]

Received 26 January 2010; revised 21 April 2010; accepted 6 May 2010; published 30 October 2010.

[1] Geological records of the history of ancient land surfaces are scarce and often fragmented by unconformities. Determining the age of these surfaces has long been the limiting factor in correlating continental paleosurfaces with marine basin deposits. Age determination of the weathering product of continental paleosurfaces as well as weathered material within the crystalline basement, is of prime importance for geodynamic reconstruction in general and more so for assessing differential dynamics between basin and basement areas, erosion rates, etc. In this paper, we examine layers of ferruginous kaolinitic paleoweathering products overlying the basement rocks of the French Massif Central. These layers, which are mainly formed in situ and are azoic (devoid of fossils), have been classically related to the "siderolithic" (Eocene-Oligocene) period because of their geographic ties with Tertiary deposits. The paleomagnetic ages of these paleoweathered surfaces have been obtained by comparing their acquired remanent magnetization, converted into paleomagnetic poles, with the APWP (apparent polar wander path) of the Eurasian plate. Recovered ages indicate late Jurassic to early Cretaceous ages (140–160 Ma with a confidence limit of 10 Ma) which are much older than the previously assumed Tertiary age. The ages obtained in this study considerably alter the present knowledge of the geodynamic evolution of the French Massif Central. Our results suggest a lack of sedimentary cover at the Jurassic-Cretaceous boundary. This implies that at the time of deposition of the siderolithic formations, the basement was cropping out and devoid of any Mesozoic cover. Furthermore, the profiles are not compacted, indicating that they have never been buried beneath a significant sedimentary cover. The obtained ages point to a great stability of French Massif Central throughout the Mesozoic, with very low ablation-erosion, while neighbouring basins (Aquitaine and Paris) were subsiding about 2000 m.

Citation: Ricordel-Prognon, C., F. Lagroix, M.-G. Moreau, and M. Thiry (2010), Lateritic paleoweathering profiles in French Massif Central: Paleomagnetic datings, *J. Geophys. Res.*, *115*, B10104, doi:10.1029/2010JB007419.

1. Introduction

[2] Records of the geological history of ancient continents are scarce, with some records totally missing, and others overwritten by successive superimposed events. This leads to preserving, in general, a patchwork of relict landforms and weathering products, discontinuous over time and space. Overcoming these difficulties is important because paleocontinents: (1) are the source material of basin deposits, (2) contribute to the study of global change through its paleoweathering surfaces formed at the interface with past atmosphere, and (3) are created through continental uplift and subsidence driven by crustal geodynamics and plate tectonics. Sedimentary basins provide, at present, the best constraints on the geodynamic evolutions of a given area. The history of a sedimentary basin's margin and basement are, on the other hand, more elusive because of weathering and erosion. However, geodynamic models of the basins could be constrained by drawing isochrones through a basin toward its marginal basement, taking into account subsidence as well as uplift and erosion at the margins. As ages of paleolandscapes are determined, erosion rate calculations become more feasible on a greater number of models with narrower time periods.

[3] The dating of paleoweathering surfaces has always been a major roadblock inhibiting progress and efforts to correlate continental formations with basin deposits. Advances in dating methods will, in the future, provide more accurate aging of continental paleosurfaces, enabling the compilation of (1) paleogeographical maps of continental weathering features and landforms and (2) stratigraphic sequences of geodynamic and climatic events in continental

[1]Mines ParisTech, Fontainebleau, France.
[2]Now at BRGM GEO/G2R, Orleans, France.
[3]Institut de Physique du Globe de Paris, Paris, France.

0148-0227/10/2010JB007419

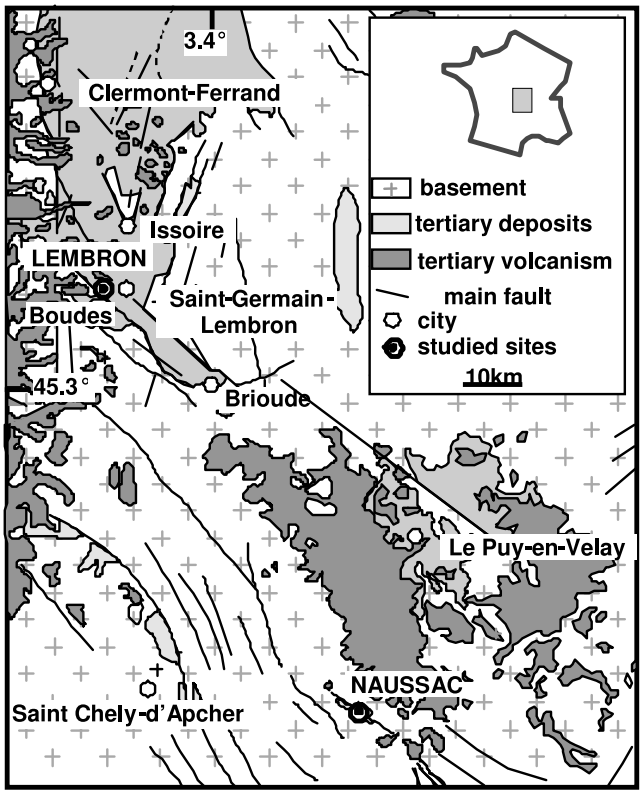

Figure 1. Geological sketch of the central part of the French Massif Central. The siderolithic formations outcrop at the edge of the Tertiary grabens. Volcanic flows cover these deposits. Sampled sites are indicated in capital letters.

settings comparable to those already available in marine settings. These compilations will provide constraints for lithospheric geodynamic models.

[4] Ferruginous paleoweathering surfaces have the potential to record the ancient geomagnetic field, thereby providing a means of age determination. In tropical soils, most of the primary remanence-carrying minerals are dissolved during weathering, and secondary magnetic minerals, such as goethite and haematite, are formed in situ [*Maher*, 1986; *Mullins*, 1977; *Schwertmann*, 1988], acquiring a crystallization or chemical remanent magnetization (CRM). The paleomagnetic pole recovered by demagnetizing the CRMs are plotted on the local apparent polar wander path (APWP) reference curve, providing an age for the paleoweathering surface.

[5] The first paleomagnetic ages obtained on lateritic soil profiles were in Australia and India: *Schmidt and Embleton* [1976] obtained Eocene and Oligocene ages for two Australian profiles. Similar studies were carried out in India by *Schmidt et al.* [1983] and *Idnurm and Schmidt* [1986]. Two paleosurfaces were defined, one of Cretaceous age, the other of Tertiary age. Other studies were carried out in Australia by *Schmidt et Ollier* [1988], *Nott et al.* [1991], and *Acton and Kettles* [1996]. The same approach has been chosen to date nodular laterites in Western Africa [*Gehring et al.*, 1992] and laterites in Guyane [*Théveniaut et Freyssinet*, 1999] and [*Théveniaut et al.*, 2007].

[6] In this paper, we will deal with paleoweathering features and remnant sedimentary deposits sitting on the basement of the French Massif Central. We first describe the geological setting; subsequently we present the results of our rock magnetic analyses aimed at identifying the remanence carriers and the results of our paleomagnetic analyses aimed at providing the ages of the weathering features. We finally discuss these ages in relation to the geodynamic evolution of the area during the Cretaceous and Tertiary periods.

2. Geological Framework

[7] Red formations related to the siderolithic facies occur in the Tertiary grabens of the French Massif Central [*Boulanger*, 1844; *de Launay*, 1892–93; *Deschamps*, 1973]. The word "siderolithic" was first used to define Tertiary ferrugineous rocks by Thurmann, a Swiss geologist, during an 1836 meeting of the French geological society in Strasbourg. Because of their richness in kaolinite and iron oxides, the red formations of the French Massif Central studied here have been identified as siderolithic, on the basis of their shared characteristics with these facies, and assigned to the Eocene-Oligocene. Their stratigraphic attribution was based on their occurrence at the edge of Tertiary graben and beneath Oligocene sediments in the grabens. Furthermore, these facies have been correlated to kaolinitic and ferrugineous continental sediments, which are widely present across all of Europe at the base of the Tertiary basins. Nevertheless, an objective analysis of the position of the red formations which cover the crystalline basement and are covered by Oligocene formations, suggests an age dating between the Trias and Oligocene.

[8] Siderolithic formations are well exposed along the fault scarp of the Limagne Graben, particularly in the Lembron area (Figure 1). These are mainly sandy and clayey fluviatile deposits of variegated colour, with only crude stratification. They display numerous paleosol features of biological (root traces, burrows, beetle nests) and mineralogical (clay illuviations, iron oxide mottles, etc.) origins. The formations are closely associated with ferruginous and kaolinitic paleosols that show some induration due to silica impregnation of clay minerals; most often they are directly overlying basement paleomorphologies and paleolandscape remnants [*Thiry and Turland*, 1985; *Thiry et al.*, 1983]. This paper describes two sites of this type, the Naussac and Lembron areas.

2.1. Naussac Area

[9] Siderolithic formations outcrop along the Naussac dam near Langogne (Lozère). Two main sections have been sampled: the first section, Naussac East, is the thickest, and the second section, Naussac West, is located about 200 m west of Naussac East and abuts a fault scarp (Figure 1).

[10] Red siderolithic formations have irregular stratification and numerous unconformities. These siderolithic beds average 0.3 to 0.8 m in thickness with fan-like arrangements that are typical of torrential debris flow deposits. In the beds, coarse sandstone facies predominate which contain irregular quartz clasts measuring from 1 cm to 10–20 cm in size that are "floating" within the red sandstone (Figure 2a). The sandstone matrix is formed of millimetric angular quartz grains. Finer and more clayey sandstones, without quartz clasts, are interbedded between the coarser sandstones and are often strongly bleached.

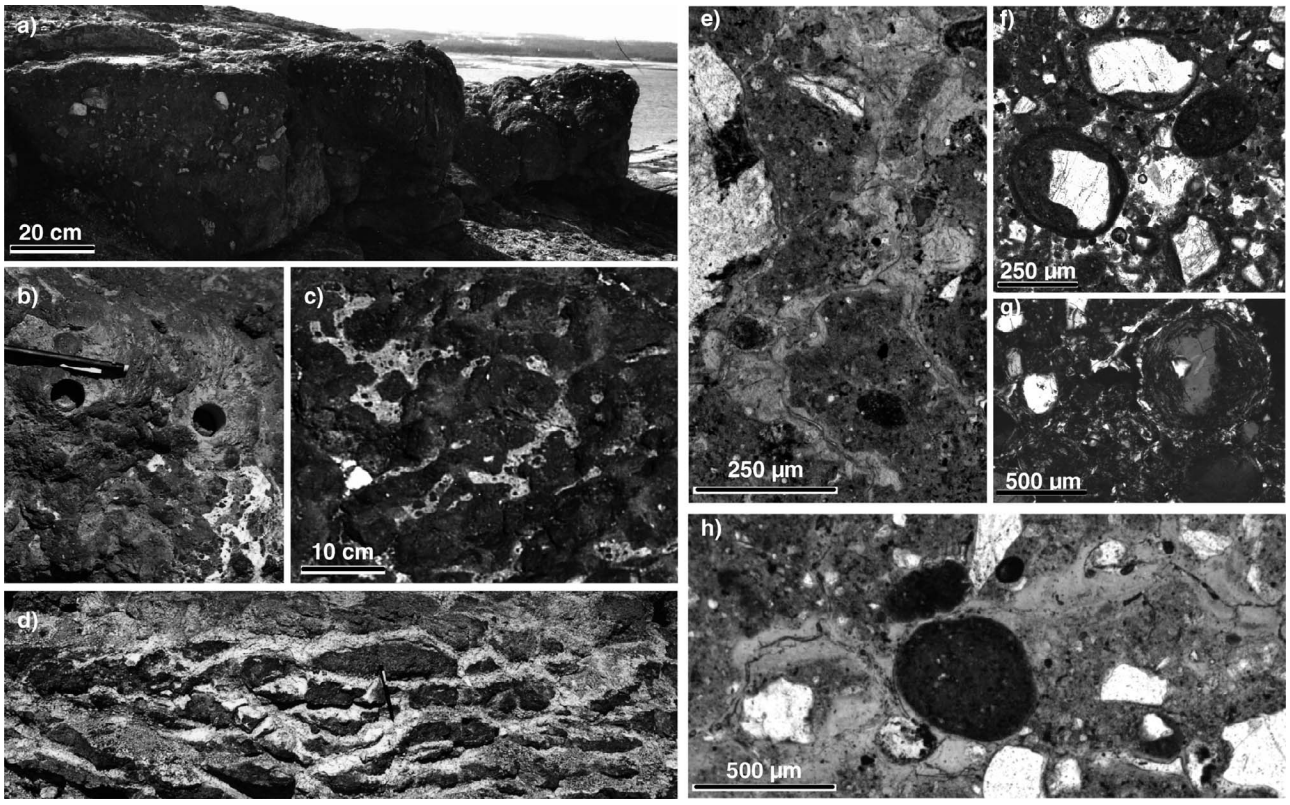

Figure 2. Naussac outcrops and thin sections: (a) Coarse sandstones with irregular stratification and angular quartz. (b) Termite burrows in red siderolithic sandstones. (c) Bleaching along termite burrows. (d) Planar joints developed in argileous levels, red sandstone bleaching comes with deposition of silica laminae. (e) Clay illuviation in cracks (plane-polarized light). (f) Granules show cores composed by quartz grains or ferrugineous matrix (plane-polarized light). (g) Granule envelopes are composed by oriented clays (cross-polarized light). (h) Ferruginous nodules in bleached matrix (plane-polarized light).

[11] Bioturbation features are prominent in some layers of the siderolithic formations. Most of these features are present in the form of crosscutting irregular burrows with centimeter-sized diameters, without particular shaping of the wall (Figure 2b). Their arrangement and configuration are those of termite burrows well known in present day soils [*Eschenbrenner*, 1986; *Wielemaker*, 1984] and in geological formations [*Genise and Bown*, 1994; *Rayot*, 1994]. Other burrows have smooth walls made of clayey material characteristic of beetle and pupate nestings [*Hasiotis*, 2003; *Martin*, 1995].

[12] The sandstone layers often display a columnar structure, formed of decimeter- to meter-sized columns demarcated with vertical joints that form a polygonal network resembling desiccation cracks. The vertical joints often show intense bioturbation and in places nodular and breccia fillings. Nevertheless, even if these joints would be primary desiccation cracks, they also would have undergone intense pedological transformations with clay illuviations, bleachings, and even silica deposits. Combined planar joints, spaced every 5 to 10 cm, develop in the clayey red sandstones. Bleaching is another noteworthy characteristic of these red sandstones. It is observed in the coarse facies along the vertical joint and in termite burrows (Figure 2c). It is also especially well developed in the planar joints. The edges of the joints are bleached and cemented with 0.1 to 2–4 mm thick laminated silica (opal-CT) (Figure 2d).

[13] The main characteristics of these red sandstones are their pedogenic microstructures. Throughout the sections there are numerous clay cutans, typical of soil horizons [*Brewer*, 1964], which result from illuviation in sandstone pores (Figure 2e), thin joints, and biological structures. Termite burrows and associated sandstone layers show a peculiar organization composed of round and ovoid granules averaging 50 to 300 μm in diameter that are formed of a quartz grain core encapsulated in oriented concentric ferruginous clay laminae (Figure 2f and 2g). These granules are probably the result of termite activity. Their internal structure, oriented coating, size, and distribution are similar to the structures described in present-day termite mounds in African soils [*Eschenbrenner*, 1988; *Wielemaker*, 1984]. The granules result from termites shaping pellets with their mandibles to remove the ground by digging burrows. The diverse bleaching features are also pedogenic or near-surface diagenetic features. Thin sections show a clear relationship between bleaching and sandstone porosity in vertical and planar as well as in the high porosity granules filling the termite burrows. Bleaching provides evidence for the iron oxide mobility (Figure 2g).

[14] The mineralogy of the red sandstones is monotonous (Figure 3a). They are almost entirely composed of quartz

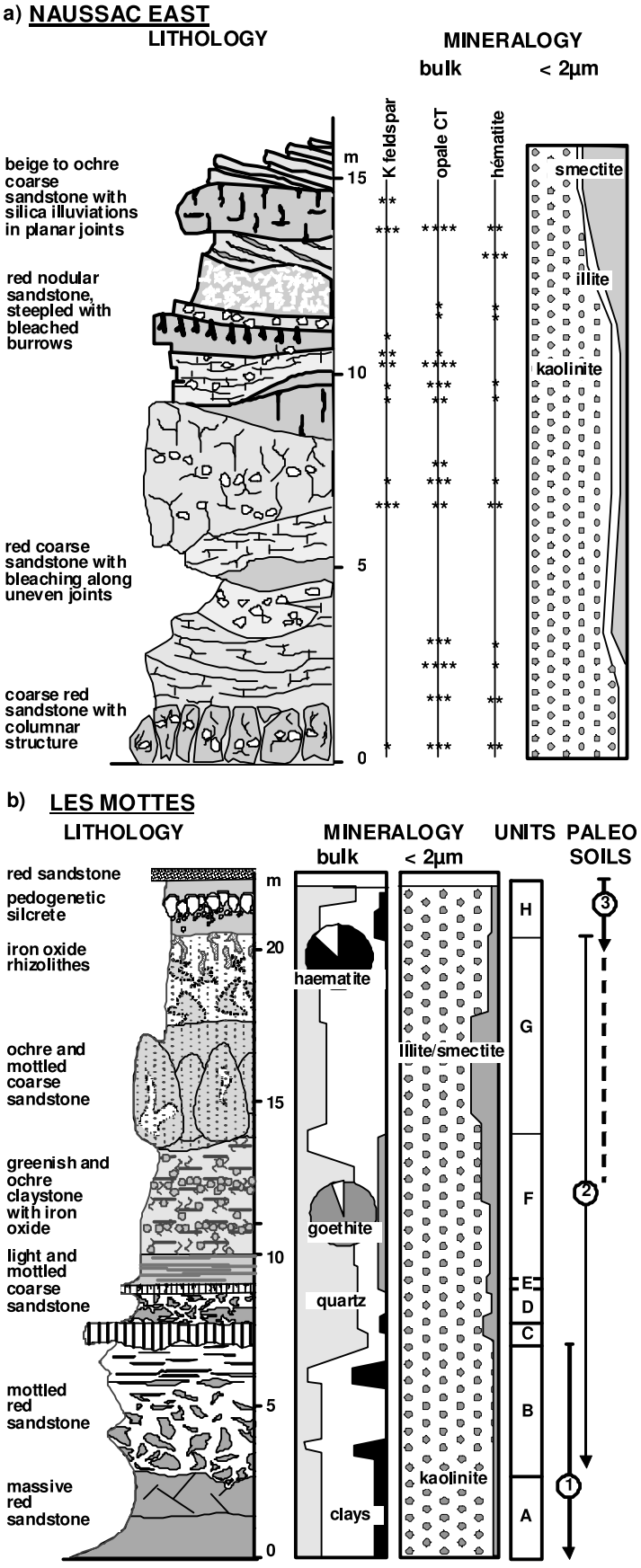
a) NAUSSAC EAST
LITHOLOGY
MINERALOGY
bulk
< 2µm
K feldspar
opale CT
hématite
smectite
illite
kaolinite
m
15
10
5
0
beige to ochre coarse sandstone with silica illuviations in planar joints
red nodular sandstone, steepled with bleached burrows
red coarse sandstone with bleaching along uneven joints
coarse red sandstone with columnar structure
b) LES MOTTES
LITHOLOGY
MINERALOGY
bulk
< 2µm
UNITS
PALEO SOILS
red sandstone
pedogenetic silcrete
iron oxide rhizolithes
ochre and mottled coarse sandstone
greenish and ochre claystone with iron oxide
light and mottled coarse sandstone
mottled red sandstone
massive red sandstone
m
20
15
10
5
0
haematite
goethite
quartz
clays
illite/smectite
kaolinite
H
G
F
E
D
C
B
A
3
2
1

Figure 3

and kaolinite, with minor content of anatase (1–2%) and sporadic K-feldspars. Iron oxides average less than 5% of the whole rock, which is mainly composed of haematite, but goethite is also present, especially near the bleached facies. Bleached facies contain opal-CT and smectite, along with kaolinite.

2.2. Lembron Area

[15] Siderolithic formations are well exposed at the southwestern edge of the Limagne graben, in the vicinity of Saint-Germain-Lembron (Puy-de-Dôme, Figure 1). There are several outcrops along the border of the graben in an area of about 3 × 2 km. The siderolithic formations are directly bound to paleolandscape features: outcropping around dome-like basement paleoreliefs, leaning against fault scarps, and infilling paleovalleys [*Ricordel*, 2007]. Paleovalley infillings are mainly formed of mottled soft sandstones and claystones, whereas monotonous red indurated sandstones rest on basement paleoreliefs. A total of 12 sections have been sampled and dated by means of paleomagnetism in this area.

2.2.1. "Les Mottes" Section

[16] The "Les Mottes" section near Boudes (Puy-de-Dôme, Figure 1) is the most representative section of the Lembron siderolithic formations. The section shows above the basement a red indurated sandstone unit overlain by mottled sands and claystones and covered by the Oligocene series of the Limagne graben (Figure 3b).

[17] The basal red sandstone is monotonous, clayey, and relatively fine-grained, without clasts and clear layering, with incipient nodular structure. The micromorphological organization is similar to those of the Naussac red sandstones. There are round and ovoid granules formed of a quartz grain core encapsulated in oriented concentric ferruginous clay laminae-like termite pellets and numerous clay cutans related to soil illuviations. This basal sandstone does not show any obvious silicification. Iron oxides stain the clays of the matrix and the granule envelopes but do not form distinctive concentrations. Haematite is the only iron oxide detected by X-ray diffraction (Figure 3b). No feldspar has been detected and kaolinite is almost the only clay mineral present, along with traces of illite and interstratified illite-smectite.

[18] Mottled red sandstones show micromorphological features similar to those of the basal red sandstone, but these sandstones are bleached and totally devoid of iron oxides in white mottles, and they are stained with iron oxides in the red mottles. This results from an alteration of red sandstone by iron oxide redistribution. There is apparently no significant change in clay mineralogy.

[19] The soft clay and sandstone units overlay the mottled sandstone across an erosional surface. They show three main units: (1) light, coarse sandstones interbedded with mottled sandstones, (2) a greenish and ochre claystone riddled with iron granules, and (3) a coarse sandstone, ochre-colored at the base and bleached in its upper part, containing iron oxide rhizoliths, which are 2 to 4 cm in diameter and up to 50 cm long. Thin sections of the units show numerous pedological features, with different kinds of clay-mineral orientations in the matrix, illuviation cutans, particularly in the higher part of the unit, and iron oxide staining the matrix or forming pisoliths with concentric fabric from 0.5 to 3 mm in diameter. The most significant pedological feature is the in situ weathering of feldspar grains into kaolinite. Illite-mica constitutes about 5% of the clay fraction besides kaolinite. K-feldspar is also present in the lower part of the unit and decreases upward until disappearing into a bleached rhizolith horizon. The iron oxides within the clayey unit are identified as goethite, whereas rhizolith features are formed by haematite. Microprobe analyses show that goethite in the pisoliths of the greenish claystone, as well as the haematite in the mottled sandstone, are substituted with aluminium, at between 5% and 15% atomic replacement. Such substitutions are generally interpreted as an indication of slightly acidic hydromorphic soil environments [*Fitzpatrick and Schwertmann*, 1982; *Muggler et al.*, 2001].

[20] A red sandstone layer containing a silcrete horizon mantles the siderolithic section below the calcareous sandstones of the Oligocene series. This upper red sandstone is also formed of round granules composed of oriented concentric ferruginous clay laminae similar to those of the lower unit. Illuviation structures develop in the pore spaces left between the granules and in larger voids and joints. A silcrete horizon about 30–50 cm thick is developed within this red sandstone. The silcrete is beige to ochre in color; it displays granules and nodules at the base, topped by columnar structures with large capping that are typical of pedogenic silcretes.

[21] The micromorphological organization distinguishes three successive superimposed paleosols (Figure 3b):

[22] 1. The basal red and mottled sandstone units are part of a first paleosol with its typical termite pellets (Figures 4a and 4b).

[23] 2. The soft clay and sandstone units have been deposited above this first paleosol and have then been weathered, leading to a well-differentiated profile with a bleached saprolite at the base, a clayey accumulation horizon with iron pisoliths, and an upper leached horizon with rhizoliths. This weathering profile develops down into the first paleosol that is partly integrated in its saprolitic horizon.

[24] 3. The sharp lower boundary of the upper red sandstone points to a probable reworking of an older paleosol (Figure 4c). This upper unit has been partly silicified by a third pedogenic event (Figure 4d).

2.2.2. Red Sandstone Sections Resting on the Basement

[25] The most common outcrops of the siderolithic formations in the Lembron area are the indurated red sandstones resting around the dome-like basement paleoreliefs. These red sandstones are massive, without any obvious stratifica-

Figure 3. Schematic lithologic sketch and clay mineralogy of the red siderolithic sandstone of (a) Naussac East section and (b) "Les Mottes" section. The red sandstones are characterized by irregular stratification, pseudo-columnar structures, planar joints, and various bleaching structures. The ferruginous facies are depicted in grey on the lithology column, the bleached facies, devoid of iron oxide, are in white. Kaolinite is almost the only present clay mineral.

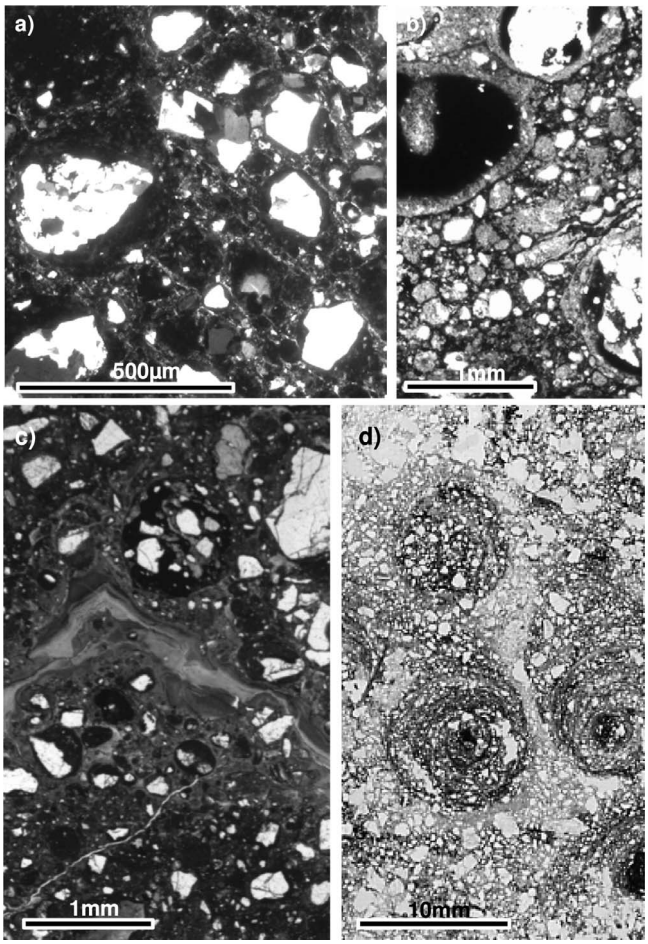

Figure 4. Micromorphology of red siderolithic formations in the Les Mottes section: (a) Granules with quartz grain cores encapsulated in ferruginous cortex (cross-polarized light). (b) Bleaching of granules in the mottled unit (plane-polarized light). (c) Pedotubule with granule infillings and illuviation cutans (plane-polarized light). (d) Nodular silcrete at the top of the section, the nodules show increasing envelopes with clear geotropism, matrix is silicified (plane-polarized light).

tion or clasts but with a centimetric incipient nodular structure exposed by weathering in areas of outcropping. Quartz and kaolinite are the main components, together with goethite and haematite and traces of anatase. The micromorphological organizations are similar to those of the basal unit of the Les Mottes section. Burrows and nodular structures are formed of round granules with concentric clay and iron oxide cutans cemented by wide clay illuviation cutans. On the other hand, in the non-bioturbed zones the granules become blurred and progressively incorporated in an unstructured red clay matrix. In places, silicification develops within and-or at the top of these red sandstones. Silicification forms flat-lying lenses or even irregular pods of porcelanite, jasper, and vitreous quartzite. They show epigenetic replacement of the mica and clay minerals by opal-CT, together with silica deposits in pores. The preservation of primary structures (bedding, burrows, mottles, etc.) and the fabrics of the enclosing rocks relate this silicification to groundwater silcretes similar to those observed in inland Australia [*Thiry and Milnes*, 1989]. The following sections: "Madriat Croix−Notre−Dame," "Madriat cemetery," "Madriat gullies," "Augnat road," "Le Letz," and "Brugères−Haute", relate to these indurated red sandstones facies.

2.2.3. Weathered Basement Sections

[26] In certain places, such as the "La Geneille" site at La Combe near St-Gervazy (Puy-de-Dôme), weathered basement sections have been preserved beneath the indurated red sandstones. The La Geneille outcrop consists of weathered, fractured, and rubefied gneiss with cracks infilled by red sandstones. The gneiss is formed of millimetric alternations of quartz beds and hardly weathered alumino-silicate (micas, orthose, plagioclase, cordierite, and sillimanite) beds. Often the gneissic structure is preserved with pedoturbation of the micaceous beds. Cracks and pedostructures display clay illuviation structures and granules with concentric ferrugineous laminae. The weathered gneiss is also silicified, with epigenic replacement of the alumino silicates by opal-CT and opal cement in the pores and joints. This silicification post-dates primary mineral weathering.

2.3. Significance of the Siderolithic Formations

[27] The paleoenvironmental and paleoclimatic interpretations of the red sandstones are not straightforward. The paleosols show some characteristics of lateritic soils (presence of kaolinite and iron oxides and absence of feldspar and mica) that may indicate tropical paleoclimates with contrasting seasons, annual monsoons, or even more pronounced humid to perhumid conditions. Termite burrows are compatible with humid environments, indicating warm temperatures. The opal-CT–bearing silicification may indicate relatively dry climatic conditions. Siderolithic red sandstones typically show ferrugineous kaolinitic paleosol features impregnated by silicification. This mineralogical sequence probably represents a shift from a humid to a dry climate.

[28] It is important to recognize the relative iron oxide mobility in these paleoprofiles, in particular in the lower saprolitic horizons, as well as in the upper leached horizons. Bleaching (iron depletion under hydromorphic conditions) accompanies silicification of the paleosol structures (joints and highly porous sandstones). This bleaching removes iron oxides and allows the formation of goethite and haematite around the bleached zones.

3. Mineralogy and Petrography

3.1. Iron Oxide Composition

[29] The bulk mineralogical composition of the red siderolithic sandstone sections is relatively monotonous and essentially dominated by quartz and kaolinite, with minor amounts of anatase and K-feldspar (Figure 3). Haematite is the only iron oxide detected by X-ray diffraction (XRD) in almost all of the samples. Goethite was only found in the clayey paleosol units, forming pisoliths. Neither maghemite nor pyrrhotite were detected in the siderolithic red sandstones.

[30] Electron microprobe analyses were performed on diverse ferruginous micromorphological features (Table 1). The paleosoil matrix and illuviation features show similar compositions: they have similar Si-Al ratios (~1.20), indicating that there is no change between the matrix and the

Table 1. Electron Microprobe Analyses of the Characteristic Structures of Red Siderolithic Sandstone[a]

	N[b]	n[c]	SiO_2	Al_2O_3	MgO	CaO	Fe_2O_3	TiO_2	K_2O	Na_2O	Total	Si/Al	Sub Al%[d]
Les Mottes													
Red matrix	6	43	35.54	25.33	0.37	0.19	22.53	0.75	1.31	0.16	86.49	1.22	_
Red illuviations	6	19	30.54	22.09	0.51	0.20	27.16	0.66	1.35	0.12	82.89	1.20	_
Orange matrix	5	38	43.03	30.09	0.33	0.16	10.02	0.94	1.37	0.09	86.07	1.23	_
Orange illuviations	5	16	42.40	30.10	0.63	0.17	8.27	0.65	2.17	0.15	84.55	1.20	_
Clear matrix	5	36	47.87	28.54	0.38	0.19	2.51	0.83	1.67	0.10	82.52	1.54	_
Clear illuviations	2	17	44.22	33.14	0.69	0.18	3.60	0.61	1.75	0.28	84.60	1.13	_
Ti-rich features	2	2	15.92	6.99	0.12	0.13	3.64	68.41	0.48	0.10	95.94	1.76	_
Fe/Ti glaebules	1	1	0.01	0.09	0.14	0.03	44.92	55.11	0.00	0.02	100.32	0.09	0.28
Haematite nodules	5	51	13.37	10.94	0.28	0.17	55.82	0.59	0.66	0.07	81.95	0.98	0.21
Goethite pisoliths	2	12	9.03	10.60	0.48	0.16	62.91	0.31	0.35	0.13	85.44	0.71	6.78
Naussac													
Red matrix	5	29	49,31	29,20	0,25	0,18	6,48	0,59	1,19	0,07	87,63	1,45	_
Red illuviations	3	13	46,11	29,67	0,45	0,18	4,76	0,41	1,24	0,19	83,29	1,32	_
Clear matrix	3	21	52,28	28,76	0,32	0,28	2,99	0,56	1,21	0,10	86,80	1,59	_
Clear illuviations	3	20	50,84	28,28	0,30	0,29	3,78	0,45	1,11	0,07	85,39	1,53	_

[a]Weight percentage composition by element; ZAF correction (atomic number (Z), absorption (A) and fluorescence (F)); 6 × 6 μm scanning zone.
[b]N, number of samples.
[c]n, number of analyses.
[d]sub Al%, percentage of Fe substituted to Al.

illuviated clay minerals. The matrix and features are more or less stained by iron oxide: Fe_2O_3 content averages around 20% in the darkest features and around 10% in the lighter parts, even dropping down to less than 3% in the bleached structures. Additionally, titanium-rich features (identified as anatase by XRD) have been detected, some of which exhibit either rhombohedral ghost crystals, corresponding to inherited oxidized ilmenite, or titanomagnetite.

[31] Haematite nodules and goethite pisoliths show a high Fe_2O_3 content (50%–60%) and are always accompanied by both alumina and silica. The Si-Al ratio of these iron-rich features is below 1, meaning there is excess alumina with respect to the kaolinite composition. Since aluminium oxides were not detected, the calculated alumina excess has to be related to aluminium substitution in iron oxides [*Correns and Engelhardt*, 1941; *Norrish and Taylor*, 1961]. Substitution ratios have been calculated under the assumption that no free silica or other clay minerals, except for kaolinite, are present in the samples. The calculation corresponds to the minimum substitution ratio. In our samples, goethite has a higher aluminium substitution for iron than haematite.

[32] Studies of present day weathering profiles show that high Al-substituted goethites (15%–30% Al) are encountered in mature soils whereas less-substituted goethites (0%–15% Al) are found in hydromorphic horizons of soils or in carbonated environments [*Fitzpatrick and Schwertmann*, 1982; *Cantinolle et al.*, 1984; *Muggler et al.*, 2001]. The authors consider haematite to be generally less substituted than goethite. A probable source of aluminium comes from the epigenesis of kaolinite by iron oxihydroxide [*Nahon et al.*, 1977].

3.2. Iron Oxide Petrography

[33] Goethite occurrence has been observed in thin sections. It occurs principally as characteristic ochre-color pigments staining illuviations. Three types of haematite have been observed in the Les Mottes section:

[34] 1. Large haematite grains (2–10 μm) that occur mostly in units A, B, and H and are scattered throughout the matrix. Some of these grains are round (Figure 5a) and clearly look like detrital grains inherited by reworking from former soils. Other grains show a dark core and a translucent outer fringe that appears like an overgrowth of an inherited grain.

[35] 2. Small rhombohedral or granular haematite crystals (<1 μm) form darker patches within the matrix, mainly in units B, C, D, and G.

[36] 3. Pigmentary haematite without any distinct crystal shape is the dominant iron oxide occurrence in the illuviation cutans of units C and D (Figure 5b).

4. Rock Magnetic Analyses

4.1. Methodology

[37] Rock magnetic analyses were performed in order to monitor any variation in magnetic mineralogy with respect to sedimentary facies of characteristic samples. The analyses were performed on the Les Mottes section, which displays all varieties of the siderolithic facies. Magnetic susceptibility was measured over the temperature range of −196°C to 700°C in order to determine unblocking-ordering temperatures and to monitor chemical transformations. The analyses were conducted at the Institut de Physique du Globe de Paris (IPGP) using two powdered samples and a KLY3 susceptibility bridge adapted with an Advanced Geoscience Instruments Company (AGICO) CS-3 furnace and CS-L cryostat. The experiments were conducted in air.

[38] Stepwise isothermal remanent magnetization (IRM) acquisition was measured on seven samples at the IPGP. The IRMs were acquired with an electromagnet in field increments ranging from 5 to 10 mT up to a maximum applied field of 1 T, using a JR5 spinner magnetometer.

[39] Magnetic hysteresis parameters are mainly controlled by mineralogy and grain size. Room temperature hysteresis loops were measured in order to test the samples homogeneity-heterogeneity. Analyses were performed at the IPGP on selected rock samples using a 2 Hz vibrating sample magnetometer in maximum fields of ±0.8 T. The sample volumes were reduced to small minicores (15 mm in diameter and 15 mm in length) for the analyses. In addition,

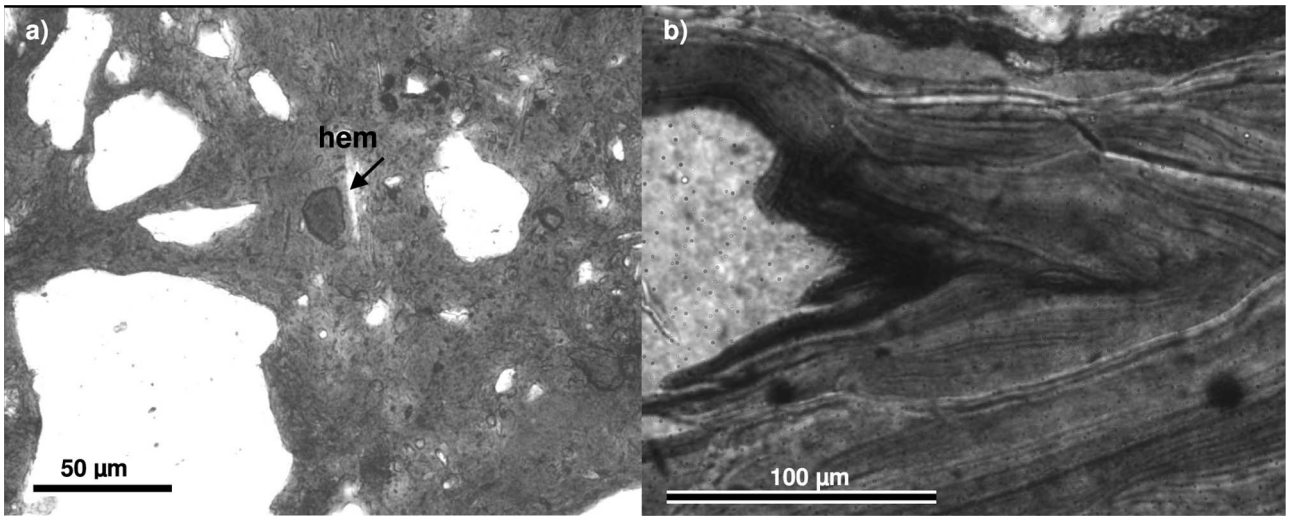

Figure 5. Micromorphological haematite features in the Les Mottes section (plane-polarized light): (a) Large haematite granule looks rounded and thus detrital (hem: haematite), sample Me6, unit A. (b) Thin haematite pigmentation in illuviations, sample, Me50, unit C.

hysteresis loops of 11 small rock chips taken mostly from the 1.5 cm^3 rock samples were analyzed at the Laboratoire des Sciences du Climat et de l'Environnement (LSCE) in Gif-sur-Yvette, France using a Princeton Measurements Corporation alternating gradient magnetometer (MicroMag™ Model 2900). Measurements on weighted rock chips (2 mm in diameter and 4–5 mm in length) were done in a maximum applied field of 1.0 T. The hysteresis parameters of all measured loops were calculated after conducting a high field slope correction aimed at subtracting the paramagnetic and-or diamagnetic signal contribution. For samples that did not reached saturation in the 0.8 T or 1 T maximum applied fields, the correction also subtracts any unsaturated antiferromagnetic contribution.

4.2. Results

[40] Thermomagnetic susceptibility experiments conducted on representative samples of the Les Mottes section units A and C are shown in Figure 6. First, the thermomagnetic curves are found to be reversible, setting aside difficulties due to heating-induced transformations during the thermal demagnetization of the remanent magnetization part of the study. Thin section petrographic observations indicate that layer A is dominated by large (2–10 μm) haematite crystals, while layer C is dominated by smaller (less than 1 μm) crystals and pigments of haematite. The reader is reminded that the stable single domain (SSD) to multidomain grain-size threshold for haematite is in the range of 15 to 20 μm and the SSD to superparamagnetism at room temperature is around 0.03 μm [*Dunlop and Özdemir*, 1997]. The progressive increase in susceptibility from room temperature to slightly above 400°C observed in unit C and not observed in unit A is compatible with a progressive unblocking of SSD particles into an unstable state (superparamagnetism) of the observed smaller grain sizes (less than 1 μm and pigmentary particles) in unit C. For a more comprehensive discussion of thermal unblocking, the reader is referred to *Néel* [1949], *Dormann et al.* [1997], and

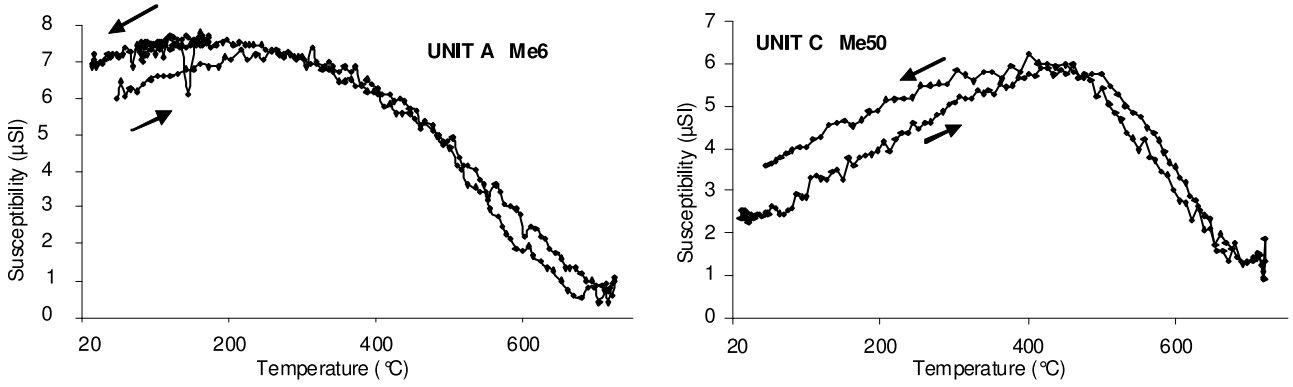

Figure 6. Susceptibility versus temperature for representative samples of the Les Mottes section units A and C. The gradual decrease in susceptibility, which shows an ordering temperature at ~650°C, reveals the presence of haematite.

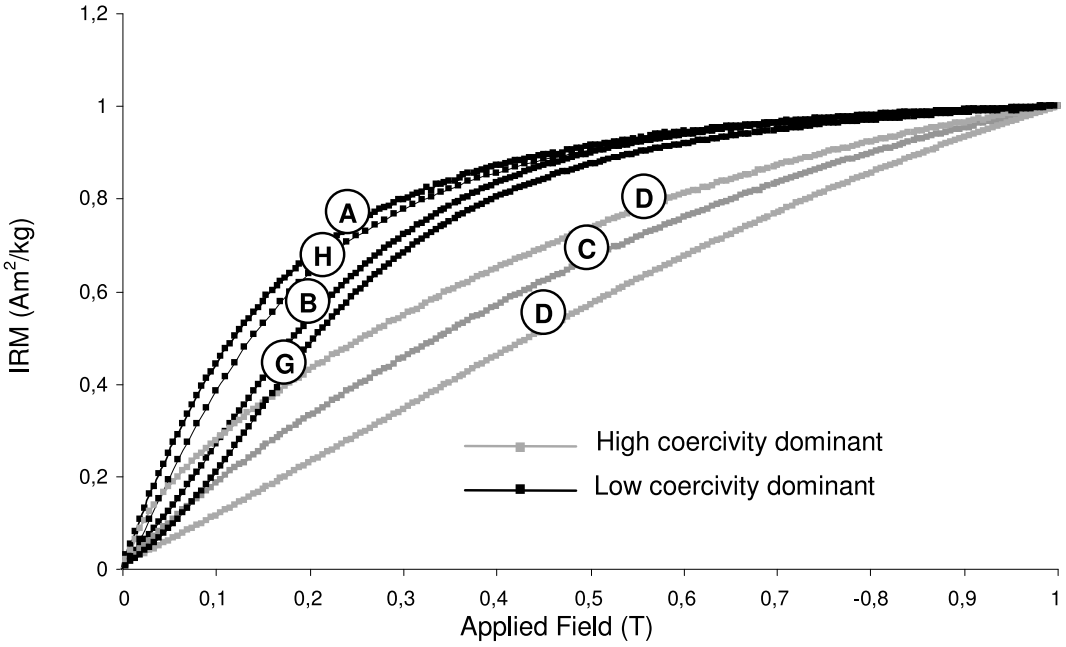

Figure 7. Isothermal remanent magnetization (IRM) curves on representative samples from the Les Mottes section. Letters refer to section units (see Figure 3). Representative curves have been normalized at 1 T.

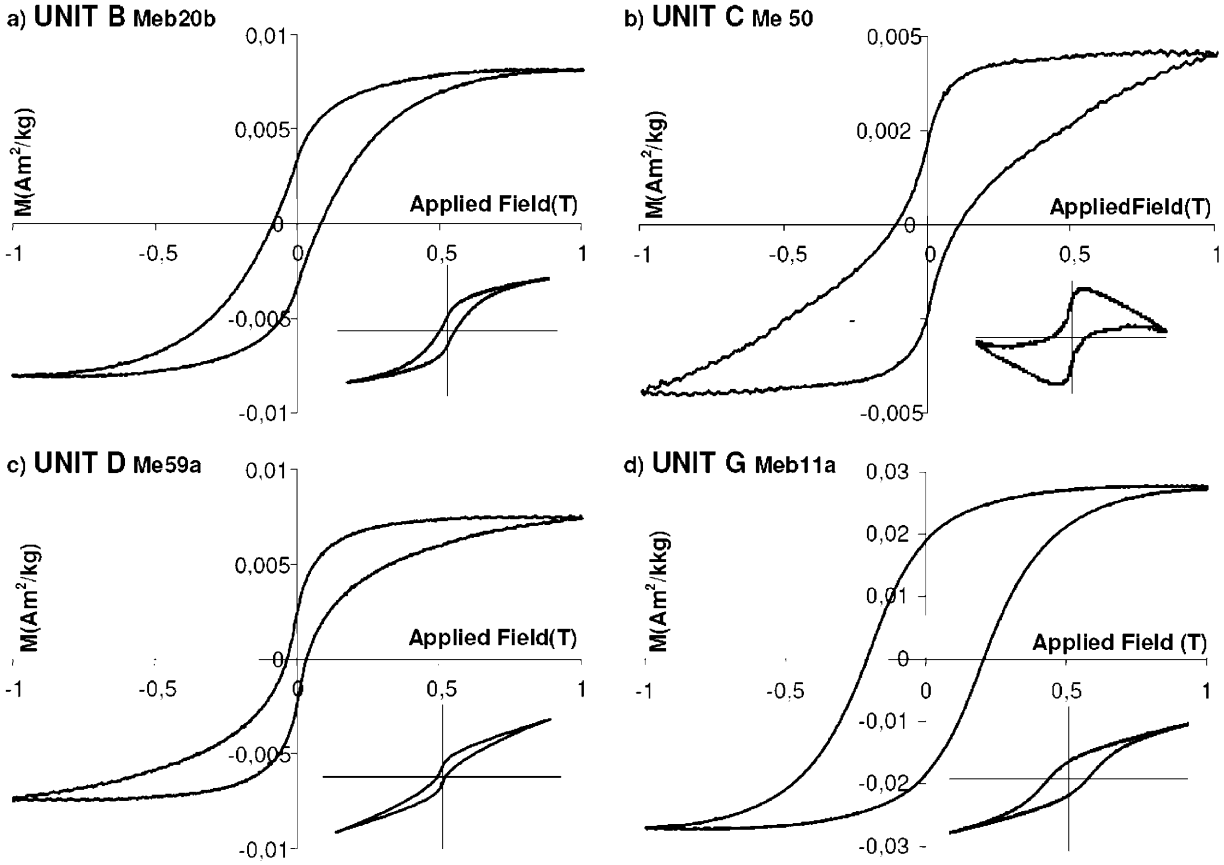

Figure 8. Hysteresis curves of selected samples of the Les Mottes section. Two types of hysteresis loops are observed: (a, b, and c) wasp-waisted hysteresis loops indicate a bimodal coercivity distribution (d) non-constricted hysteresis indicate a unimodal coercivity distribution. The small insets show the uncorrected hysteresis loop.

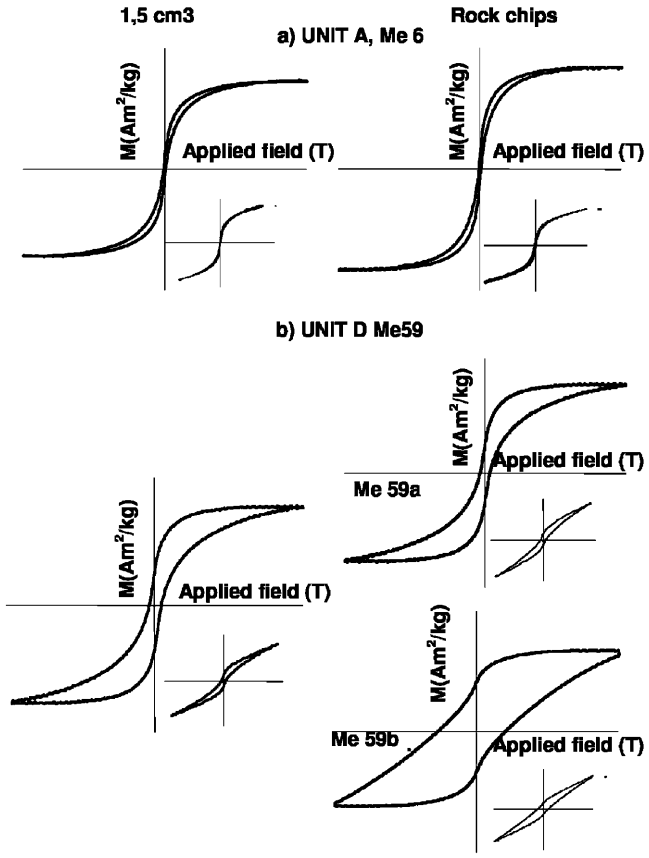

Figure 9. Comparison of hysteresis loop shapes between the 1.5 cm^3 samples and the subsampled rock chips. Distribution of iron oxide phases is homogeneous in unit A and heterogenous in unit D.

Dunlop and Özdemir [1997]. Both thermomagnetic curves show complete magnetic disordering above 650°C. This is consistent with haematite. Evidence for goethite disordering around its Néel temperature of 120°C for stoichiometric goethite or lower temperatures in the case of Al-substituted goethite is not observed.

[41] The IRM acquisition curves for representative samples from Les Mottes section units A, B, C, D, G, and H, are plotted in Figure 7 and normalized to their IRM acquired in a 1 T magnetic field. The six samples depict two types of behavior. Units A, B, G, and H (units where pigmentary haematite has not been identified through petrographic observations) display an initial rapid IRM acquisition up to about 300 mT followed by gentle acquisition slope up to 1 T. Saturation is almost, but not completely, achieved by the maximum field applied. IRM acquisition curves of units C and D, the only units where pigmentary haematite was observed, show a monotonic increase in IRM acquisition up to the maximum 1 T field applied. Saturation is not achieved, and the shape of the curve suggests that saturation is not eminent but occurs at much higher fields. Given the petrographic observations, it seems reasonable to conclude that the very fine grained pigmentary haematite is the mineral component displaying the highest coercivity. Increasing coercivity of remanence with decreasing haematite particle size is an observed trend [e.g., *Peters and Dekkers*, 2003, and references therein]. We can therefore deduce that the two acquisition slopes in the IRM acquisition curves of units A, B, G, and H are evident because of coarser (high slope–low coercivity section) and finer (lower slope–higher coercivity section) crystalline haematite.

[42] Hysteresis loops display the average behavior of a bulk material. Figure 8 shows the results of representative samples from units B, C, D, and G. Samples from units containing no pigmentary haematite display nonconstricted (Figure 8d) to slightly wasp-waisted (Figure 8a) loops. Consistent with the IRM acquisition data, these samples are saturated or nearly saturated. Units C and D show the most pronounced wasp-waisted loops because there are two distinct populations with contrasting coercivities. It is also these samples, containing the observed pigmentary haematite, that show a greater heterogeneity in magnetic behavior with sample size (see Figure 9).

5. Paleomagnetism

5.1. Methodology

[43] Weathering profiles were sampled in vertical intervals of 40–50 cm by taking minicores (25.4 mm in diameter and 3–8 cm in length) with a gasoline-powered portable drill equipped with a water-cooled diamond bit. Paleomagnetic minicores were oriented by sun and-or magnetic compasses. They have been cut in the laboratory into standard specimens measuring 2.2 cm × 2.5 cm. Clay-rich intervals were not sampled because they displayed sliding joints.

[44] All remanence measurements were carried out in the IPGP paleomagnetic laboratory using a three-axis, 2 G cryogenic magnetometer, and the results were interpreted using the PaleoMac 5 software [*Cogné*, 2003]. In total, 410 samples were analyzed for this study. The samples were subjected to stepwise (50°C–10°C increment) thermal demagnetization up to maximal temperatures between 650° C and 700°C. Magnetochemical changes were monitored by measuring the low-field susceptibility after each demagnetization step. Results of the progressive demagnetization experiments were displayed using the orthogonal Zijderveld diagrams [*Zijderveld*, 1967]. Characteristic components were determined by principal component analysis, with lines constrained (or not) passing through the origin [*Kirschvink*, 1980]. During progressive demagnetization, when directions fit a great remagnetization circle in equal-area projection, the parameters of this circle were calculated with the *McFadden and McElhinny* [1988] method. Statistical procedures were used to calculate site-mean directions and paleomagnetic poles following the *Fisher* [1953] method or the McFadden and McElhinny method in case that great circles were defined. Paleomagnetic results are described in terms of components and characteristic directions. When necessary, we first calculated a tentative mean direction by including all samples from the individual unit. Subsequently, we rejected specimens diverging more than 30° from this mean, providing that the direction be calculated on fewer than four steps or with mass analyzer detector (MAD) values greater than 12°. The mean paleomagnetic directions have been calculated as discussed hereafter and are presented in Table 1. Our procedure explains why variable *n*

Table 2. Mean Paleomagnetic Directions and Paleomagnetic Poles From the Different Sections Analyzed in the French Massif Central[a]

Site	Lat. (°N)	Long. (°E)	*N*	*n*	*D*	*I*	*k*	α_{95}°	VGP Lat. (°N)	VGP Long. (°E)	dp	dm°
Naussac												
Naussac East	44.72	3.85	22	15	12.5	45.7	23.3	8.4	69.8	150.1	6.8	10.7
Naussac West	44.72	3.85	15	9	16.3	46.1	54.3	7.1	68.4	141.3	5.8	9.0
Mean	44.72	3.85	2	2	14.4	45.9	1790	5.9	69.1	145.5	4.8	7.5
Lembron												
Augnat inselberg	45.42	3.2	14	8	359.0	60.5	109.2	5.4				
Madriat gullies	45.43	3.2	17	15	3.5	58.1	60.4	5.0				
Croix Notre Dame	45.43	3.2	7	7	4.2	58	119	5.6				
Mottes unit A	45.47	3.2	18	17	358.8	57.6	65.1	4.5				
Mottes unit B	45.47	3.2	18	15	3.8	63.2	44.4	5.8				
Mottes unit C	45.47	3.2	21	9	168.9	−46.5	120.5	4.7				
Mottes unit D	45.47	3.2	15	13	170.8	−25.4	51.4	5.8				
Mottes unit E	45.47	3.2	7	6	176.0	−39.7	101.7	6.7				
Mottes unit G	45.47	3.2	25	7	171.2	−47.5	188.7	4.0				
Mottes unit H	45.47	3.2	3	3	354.5	57.5	223.1	8.3				
Les Mottes GC	45.47	3.2	7	7	257.2	6.1	-	9.8				
Vallée des Saints	45.47	3.2	17	8	353.7	47.5	49.9	8	72.5	201.9	6.7	10.4
Augnat Road	45.42	3.2	10	8	357.4	48.3	52.9	7.7	73.7	191.2	6.6	10.1
Le Letz	45.43	3.2	11	5	354.5	50.4	76.9	8.8	75.1	202.1	7.9	11.8
Brugères Hautes	45.43	3.2	13	8	354.0	49.7	47.7	8.2	74.4	202.8	7.3	10.9
Madriat Cemetery	45.43	3.2	12	8	2.8	46.4	33.4	9.7	72.2	175.1	8.0	12.5
La Geneille	45.45	3.25	19	15	161.7	−52.8	102	3.7	71.5	238.8	3.5	5.1
Mean	45.4	3.2	6	6	356.3	50.0	279.2	4.1	75.7	195.7	3.7	5.5

[a]Sites in italic show a mean direction close to the recent IGRF direction; Lat. (°N), site latitude; Long. (°E), site longitude; *N*, number of studied samples; *n*, number of samples used for the mean; *D*, declination; *I*, inclination; *k*, precision parameter; α95, 95% confidence cone around the mean direction; VGP Lat (°N), virtual geomagnetic pole latitude; VGP Lon. (°E), virtual geomagnetic pole longitude; dp and dm, errors around the pole position.

specimens, used for computing the mean, are often smaller than the variable *N* cores measured for a site.

5.2. Results

5.2.1. Naussac Sites

[45] Two sites, Naussac East and Naussac West, have been sampled in the southern Massif Central region. In total, 28 samples were treated on the eastern site and 15 samples were treated on the western site (Table 2). The natural remanent magnetization (NRM) ranges from 0.1 to 10 mA/m, depending mainly on the degree to which the samples are altered by bleaching. Most of the magnetization signal is removed between the temperature steps of 580°C and 645°C, indicating that haematite is a magnetic carrier (Figures 10a and 10d). Demagnetization is nearly univectorial between 420°C and 630°C for directions of normal polarity and between 180°C and 630°C for reverse polarity directions. The characteristic directions are listed in Table 2 and plotted in Figures 10b and 10e. The directions are grouped into two antiparallel clusters. The mean magnetization direction of the Naussac East profile, derived by combining the normal and reversed directions, shows a declination of 12.5° and an inclination of 45.7°, with α95 values of 8.4°. The mean magnetization direction for Naussac West is declination, 16.3°; inclination, 46.1°; and α95, 7.1°.

5.2.2. Lembron Area

[46] Twelve sites have been sampled in the Lembron area. Two sites, "Saint Gervazy Castle" and "Bards," were rejected because their magnetization directions remained random after data cleaning, preventing the calculation of a representative mean direction. Neither the geological setting nor the petrographic characteristics can explain the randomness of the magnetization directions recovered from these sites. Dispersion may be related to successive overprints over the duration of their geological evolution. Three other sites, "Augnat Inselberg," "Madriat Croix Notre Dame," and "Madriat Gullies," were also rejected because their mean characteristic high temperature components were close to the International Geomagnetic Reference Field (IGRF) direction. These sites may have been overprinted recently. The Les Mottes section has been subdivided into subunits showing different paleomagnetic behavior. Representative progressive demagnetization, characteristic and mean directions of each subunit are plotted in Figure 11. For the other Lembron sites, representative progressive demagnetization, characteristic and mean directions are plotted in Figure 13. All mean characteristic directions are reported in Table 2.

5.2.2.1. Les Mottes Section

[47] Haematite appears as the main magnetic carrier. Characteristic directions carried by haematite have been identified in all units from the base to the top. The magnetizations of units A and B become unstable in the 550°C – 630°C range (Figures 11a and 11c). Unit A directions are all of normal polarity and the computed mean direction is close to the recent IGRF direction (Figure 11b). The mean direction of unit B is similar to that of unit A, but here both polarities are observed (Figure 11d). A high temperature component is removed in units C, D, E, and G between 630°C and 670°C (Figures 11e, 11g, 11i, and 11k). Characteristic directions obtained in these units are all of reverse polarity. Mean characteristic directions are similar for units C, E, and G. Unit D shows the same behavior but inclination differs (Figure 11f). Unit H exhibits similar behavior to that of units A and B, where the mean characteristic direction is close to the IGRF (Figures 11m and 11n). Mean characteristic directions for the Les Mottes section are plotted in Figure 12. Mean characteristic directions (Les Mottes units A, B, and H) are close to the recent IGRF direction. Mean characteristic directions (Les Mottes units C, D, E, and G)

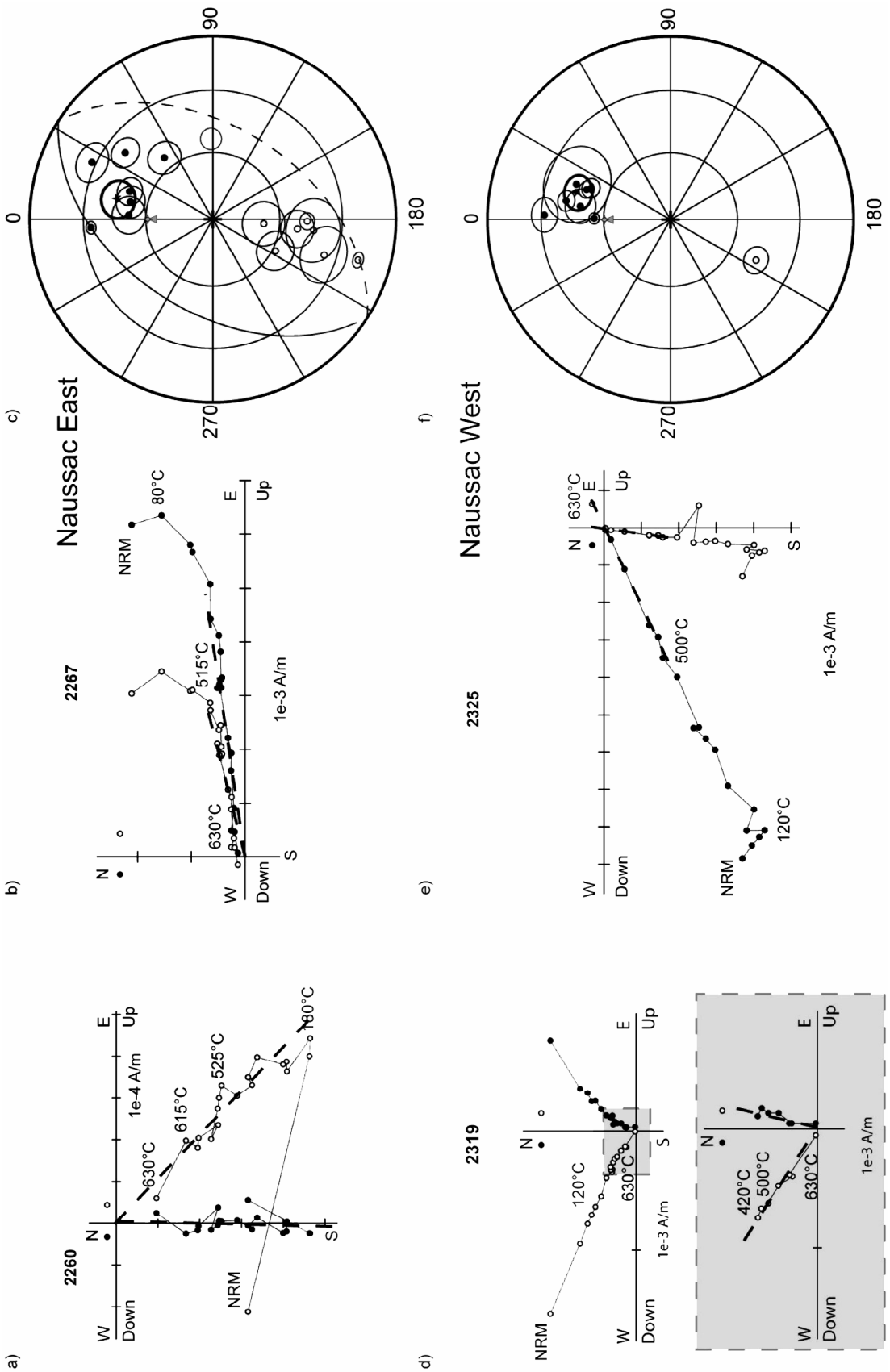

Figure 10. Representative orthogonal projection plots for thermal demagnetization of (a, b) Naussac East and (d, e) Naussac West. A zoom on the orthogonal plot of sample 2319 is presented in Figure 10d.The closed (open) symbols refer to the horizontal (vertical) plane. Equal area projection of high temperature characteristic component in Naussac East (Figure 10c) and Naussac West (Figure 10f): small star represent the mean direction with its 95% confidence circle. Closed (open) symbols refer to directions in the lower (upper) hemisphere. Grey crosses represent the IGRF (International Geomagnetic Reference Field) (declination: –0.5°; inclination: 60.5°) and grey triangles the GAD (geocentric axial dipole) (inclination: 63.2°).

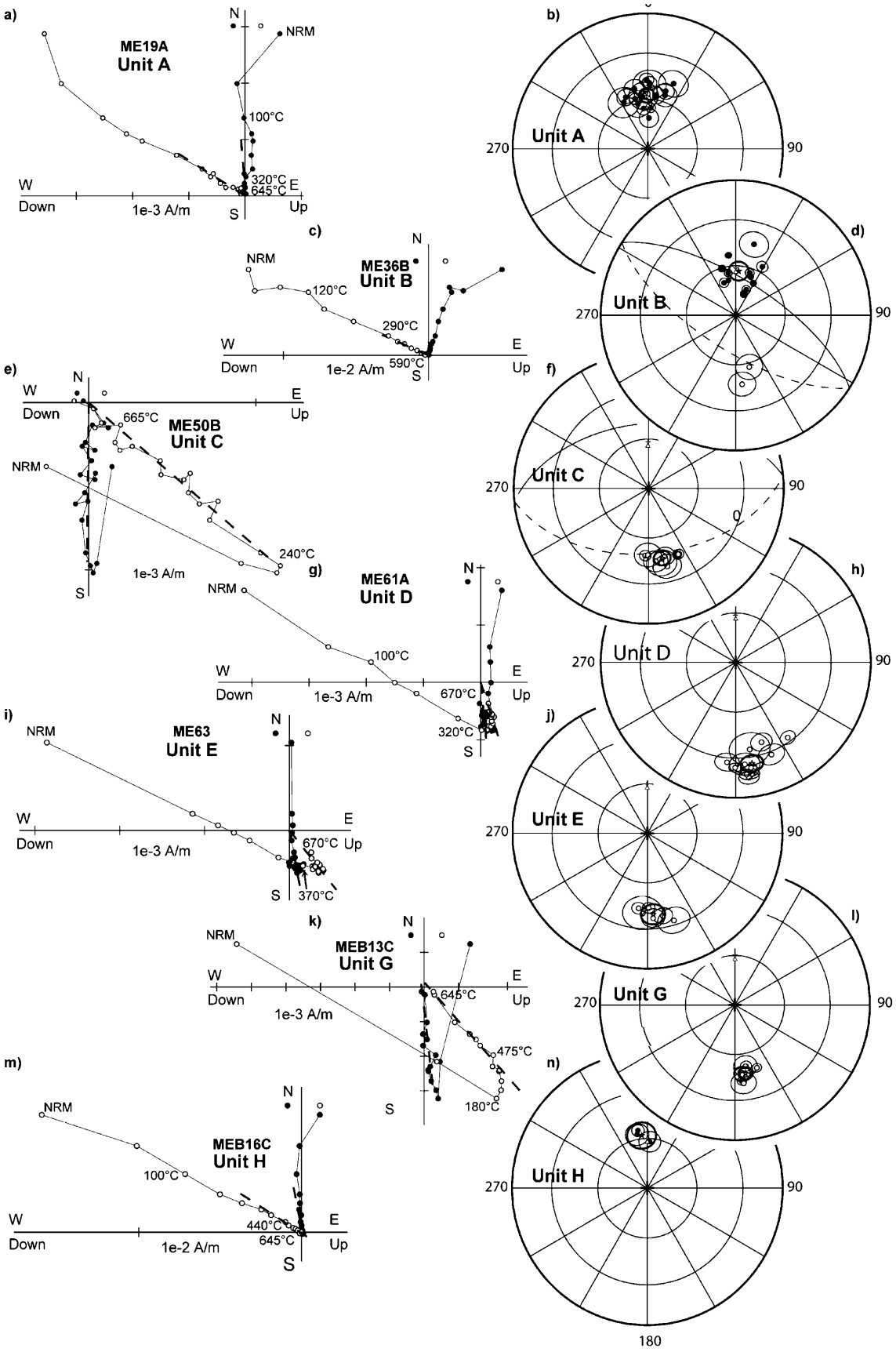
a)
ME19A
Unit A
N
NRM
100°C
320°C
645°C
W
E
Down
1e-3 A/m
S
Up
b)
Unit A
270
90
c)
NRM
ME36B
Unit B
120°C
290°C
590°C
W
E
Down
1e-2 A/m
S
Up
d)
Unit B
270
90
e)
W
E
Down
665°C
Up
ME50B
Unit C
NRM
240°C
1e-3 A/m
S
f)
Unit C
270
90
g)
ME61A
Unit D
NRM
100°C
W
E
Down
1e-3 A/m
670°C
320°C
Up
S
h)
Unit D
270
90
i)
NRM
ME63
Unit E
W
E
Down
1e-3 A/m
670°C
Up
S
370°C
j)
Unit E
270
90
k)
NRM
MEB13C
Unit G
W
E
Down
645°C
Up
1e-3 A/m
475°C
S
180°C
l)
Unit G
270
90
m)
NRM
MEB16C
Unit H
100°C
W
E
Down
1e-2 A/m
440°C
645°C
Up
S
n)
Unit H
270
90
180

Figure 11

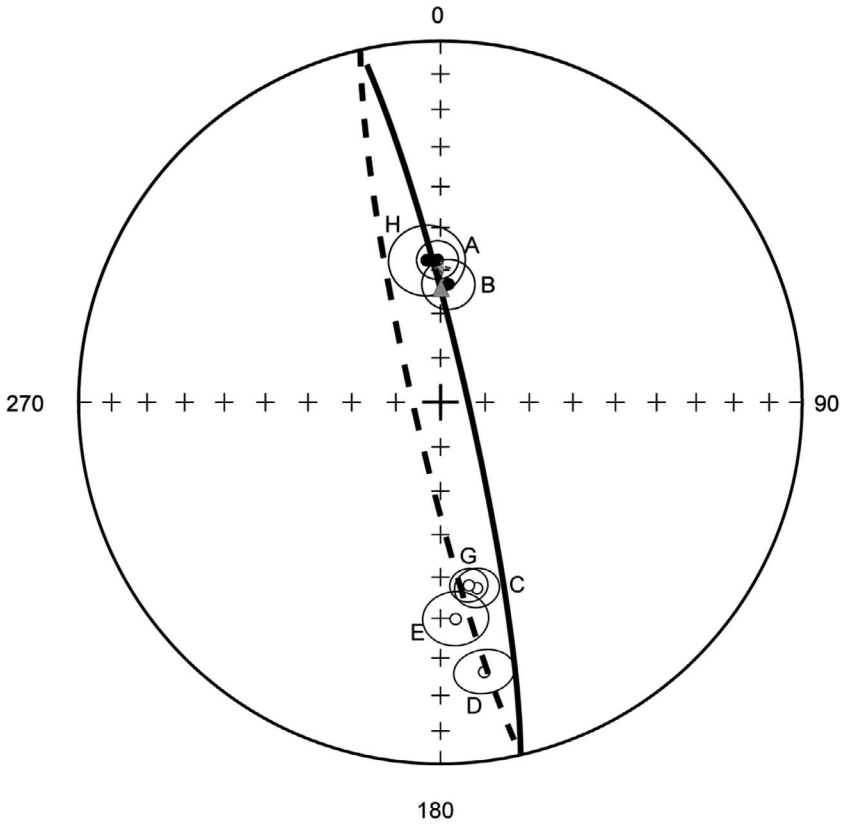

Figure 12. Equal-area projection of mean characteristic directions for Les Mottes units. Directions are fitting a great circle. Small stars represent the mean direction with its 95% confidence circle. Closed (open) symbols refer to directions in the lower (upper) hemisphere. Grey crosses represent the IGRF (declination: -0.7°; inclination: 61.2°) and grey triangles the GAD (Inclination: 63.8°).

are different. In terms of equal-area projection, the mean directions fall along a great circle path, quite well defined, which cross the IGRF direction. This may be related to the superimposition of two magnetization signals, one being of recent age, the other of older age. The unit mean characteristic direction and great circle for the Les Mottes section are summarized in Table 2.

5.2.2.2. "Vallée des Saints"

[48] Only 8 samples out of 17 show stable characteristic directions. The initial remanence ranges from 0.1 to 8 mA/m depending on the degree of bleaching of the samples. Both polarity directions are recorded by characteristic remanence vectors unblocking at between 580°C and 650°C, which we attribute to haematite (Figure 13a). Characteristic directions are plotted in Figure 13b and listed in Table 2. They group tightly into two antipodal clusters. The mean magnetization is declination, 353.7°; inclination, 47.5°, and α95, 8°.

5.2.2.3. "Augnat Road" Section

[49] This section gave a much better sample score with 8 samples from 10 characteristic directions which deviated less than 30° from the calculated mean direction. Most of the demagnetization occurs in the haematite temperature range at between 580°C and 610°C (Figure 13c). The high temperature components are all of normal polarity (Figure 13d). The mean direction has a declination of 357.4°, an inclination of 48.3°, and α95 of 7.7° (Table 2).

5.2.2.4. "Le Letz" Section

[50] Eleven samples were successfully analyzed using thermal demagnetization. Most of the demagnetization occurs at temperature steps above 600°C (Figure 13e). The magnetic carrier is haematite. Six samples were rejected because no high temperature component could be identified. The mean direction computed is declination, 354.5°; inclination, 50.4°; and α95, 8.8° (Figure 13f and Table 2).

5.2.2.5. "Brugères Haute" Section

[51] Twelve samples were treated for the "Brugères Haute" site. Even if directions are poorly defined above 400°C (Figure 13g), straight lines can be forced to pass through the origin [*Kirschvink*, 1980]. Despite the high background noise, we assumed it was possible to isolate

Figure 11. Representative orthogonal projection plots for thermal demagnetization from the different units of the Les Mottes section (closed (open) symbols refer to the horizontal (vertical) plane) and equal area projection of high temperature characteristic components. Small stars represent the mean direction with its 95% confidence circle. Closed (open) symbols refer to directions in the lower (upper) hemisphere. Grey crosses represent the IGRF (declination, −0.7°; inclination, 61.2°) and grey triangles the GAD (inclination, 63.8°).

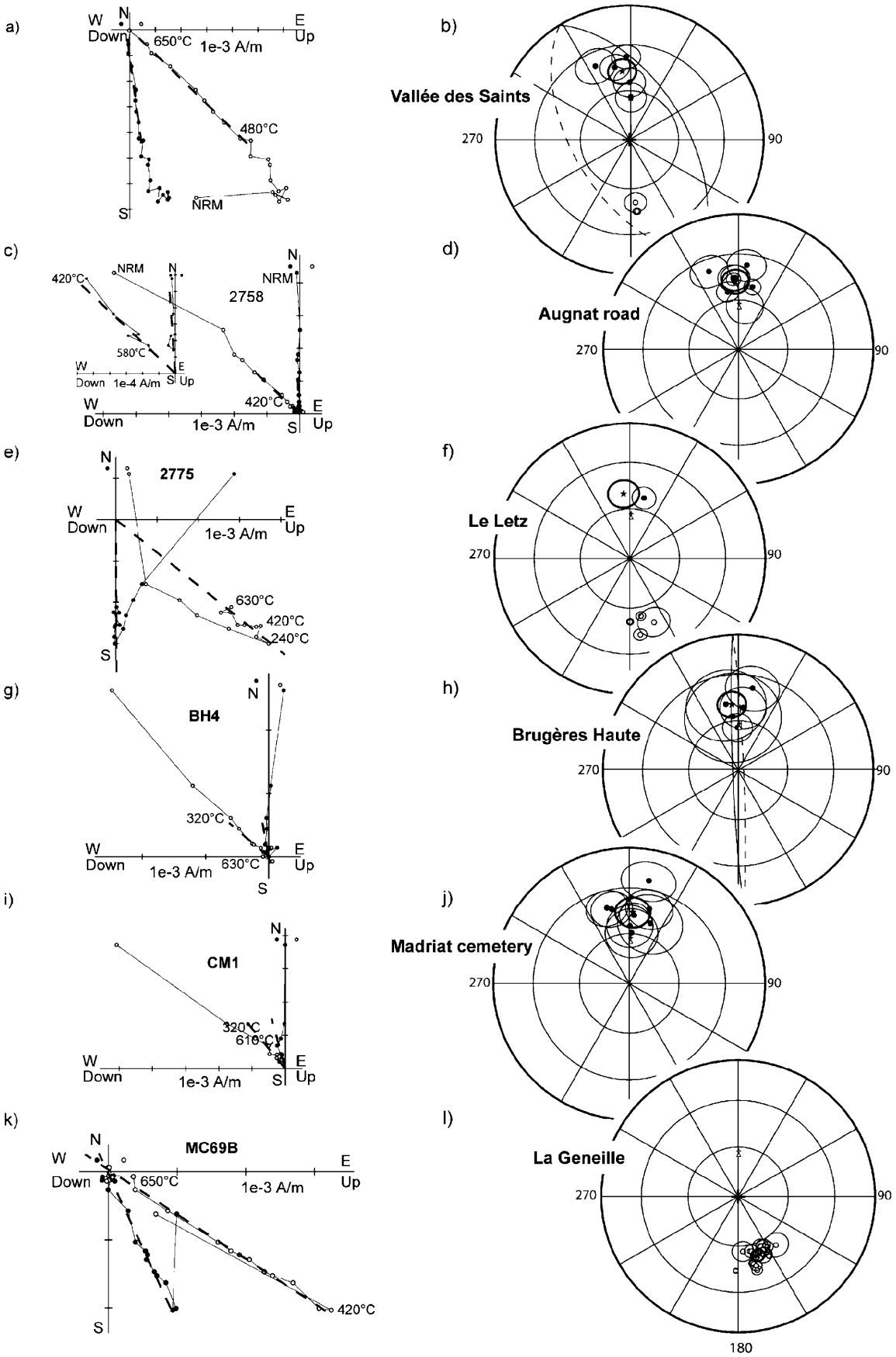
a)
N
W
E
Down
650°C
1e-3 A/m
Up
480°C
NRM
S
b)
Vallée des Saints
270
90
c)
NRM
N
420°C
NRM
2758
580°C
W
E
Down
1e-4 A/m
S
Up
W
420°C
E
Down
1e-3 A/m
S
Up
d)
Augnat road
270
90
e)
N
2775
W
E
Down
1e-3 A/m
Up
630°C
420°C
240°C
S
f)
Le Letz
270
90
g)
N
BH4
320°C
W
E
Down
1e-3 A/m
630°C
Up
S
h)
Brugères Haute
270
90
i)
N
CM1
320°C
610°C
W
E
Down
1e-3 A/m
S
Up
j)
Madriat cemetery
270
90
k)
N
MC69B
W
E
Down
650°C
1e-3 A/m
Up
420°C
S
l)
La Geneille
270
90
180

Figure 13

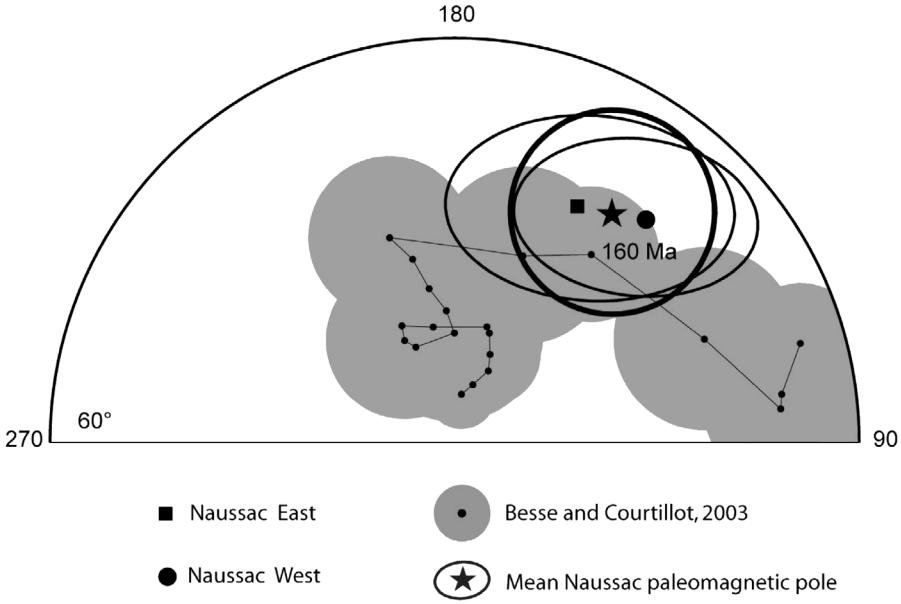

Figure 14. Paleomagnetic poles obtained in the Naussac area compared to the 0–200 Ma apparent polar wander path (APWP) Eurasia [*Besse and Courtillot*, 2003]. Mean Naussac paleomagnetic pole is close to the 160 Ma pole of the Eurasian APWP.

characteristic directions for 60% of the samples, even if the MAD was as great as 30° (Figure 13h). The mean isolated direction has a declination of 354.0°, an inclination of 49.7°, and α95 of 8.2° (Table 2).

5.2.2.6. "Madriat Cemetery" Section

[52] Twelve samples were treated. Consistent with the results from the Brugeres Haute site, the obtained directions are poorly defined above 400°C for most of the samples (Figure 13i). Eight characteristic directions carried by haematite were obtained by forcing straight lines to pass through the origin (Figure 13j). The mean direction obtained is declination, 2.8°; inclination, 46.4°; and α95, 9.7° (Table 2).

5.2.2.7. "La Geneille" Section

[53] The La Geneille site is based on three distinct profiles. The initial remanence ranges from 0.5 to 25 mA/m. Thermal demagnetization shows nearly straight line demagnetization between 120°C and 660°C, with a sharp decrease in intensity above 630°C (Figure 13k). These characteristic components are carried by haematite, as most of the demagnetization occurs above 600°C. All of the characteristic directions are well clustered and show a reverse polarity (Figure 13l). The mean direction obtained is declination, 161.7°; inclination, −52.8°; and α95, 3.7°.

6. Summary of Paleomagnetic Data

[54] Tentative dating is based on the assumption that a site mean direction could be transformed into a paleomagnetic pole and compared with the well-calibrated Eurasian APWP [*Besse and Courtillot*, 2002, 2003]. Paleomagnetic poles calculated for the two sites of Naussac are reported in Table 2 and in Figure 14. The mean paleopole position plots on the late Jurassic portion of the Eurasian APWP, with the confidence ellipse of 95% overlapping the 160 Ma reference pole (Figure 14).

[55] All average paleomagnetic poles obtained from the different sampled areas in the Lembron area are plotted in Figure 15. Although the distribution is not really Fisherian, a mean paleomagnetic pole has been calculated for the Lembron area. The calculated mean paleopole position is plotted on the 140 Ma reference pole, with margin of error covering a period of 10 Ma.

[56] Looking site by site, it appears that apart from the La Geneille and Madriat Cemetery sites, all paleomagnetic poles fall on the reference Eurasian APWP and are close to the 140 Ma pole. First of all, there is no reason to apply any bedding correction for these sites. The Madriat Cemetery site pole does not fall on the reference APWP, but its ellipse of confidence overlaps with the APWP curve. The distribution could suggest local vertical axis rotations. The La Geneille site paleomagnetic pole is statistically different from the mean Lembron area paleomagnetic pole according to the *McFadden* test [1982]: $\gamma c = 6.4°$ and $\gamma 0 = 10.2°$.

[57] Two hypotheses are put forward for the La Geneille site: a rotation of the site around a vertical axis of 13° ± 11° or a westerly tilt around a northwesterly axis. Neither the regional structures nor field observations can adjudicate for

Figure 13. Representative orthogonal projection plots for thermal demagnetization from the different sections of the Lembron area (closed (open) symbols refer to the horizontal (vertical) plane) and equal area projection of high temperature characteristic components. Small stars represent the mean direction with its 95% confidence circle. Closed (open) symbols refer to directions in the lower (upper) hemisphere. Grey crosses represent the IGRF (Declination: −0.7°; Inclination: 61.2°) and grey triangles the GAD (Inclination: 63.8°).

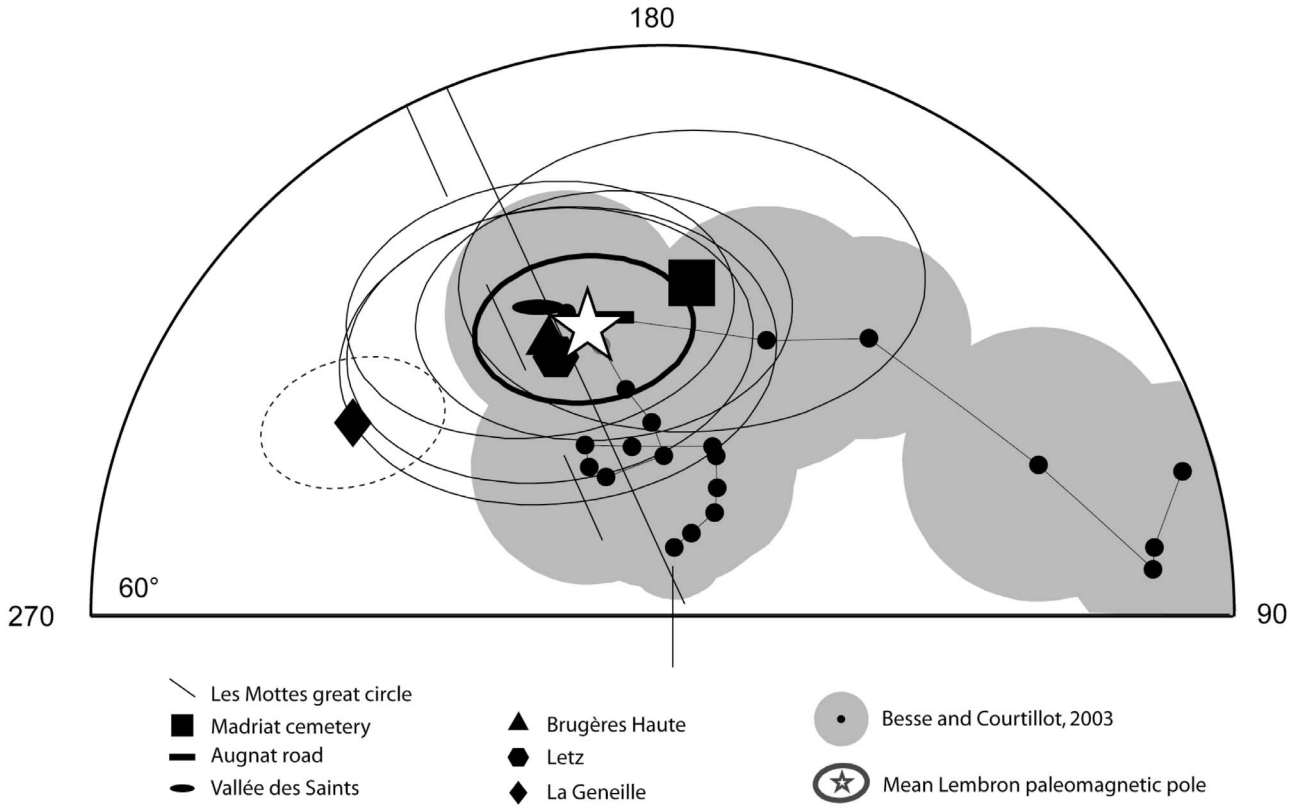

Figure 15. Paleomagnetic poles obtained in the Lembron area compared to the 0–200 Ma APWP of Eurasia [*Besse and Courtillot*, 2003]. *McFadden* [1982] test is negative comparing "La Geneille" Paleomagnetic pole and mean Lembron paleomagnetic pole. Mean paleomagnetic pole is close to the 140 Ma pole of the Eurasian APWP.

one hypothesis or the other. Therefore, the La Geneille site data have been excluded to calculate the mean paleomagnetic pole for the Lembron area (Figure 15). The paleopole position is plotted on the 140 Ma reference pole, with its margin of error covering a period of 10 Ma.

[58] The late Jurassic to early Cretaceous ages obtained in this study are quite different from the Eocene-Oligocene age previously inferred for "siderolithic" red sandstones. But it has to be emphasized that there is not any paleontological or geometrical constraint that is inconsistent with this dating. Moreover, recent paleomagnetic and radiometric dating revealed that numerous kaolinitic and ferruginous formations, which classically were ascribed to Tertiary ages, date back to the Lower Cretaceous period. This is the case for the deep kaolinitic profiles on the Hercynian basement in the Belgian Ardenne [*Yans*, 2003; *Thiry et al.*, 2006] and also for the siderolothic iron ore deposits in the eastern Paris Basin [*Théveniaut et al.*, 2007]. Additionally, the Bonherz iron ore deposits in the paleokarsts developed on the Jurassic limestone platform of the Paris Basin also have to been reconsidered as dating to the Cretaceous age, as well as paleokarst deposits in the southern Massif Central [*Thiry et al.*, 2006].

[59] These datings emphasize the major lateritic event that developed during the Early Cretaceous age due to sea level drops, wide dewatering, and peculiar paleoatmosphere with very high CO_2 content [*Berner and Kothavala*, 2001]. This major lateritic event is not restricted to Europe but is also well known in North America (up to Canada), South America (down to Argentina), and in Australia.

7. Conclusion

[60] Paleomagnetic data from the in situ paleosols of the Naussac and Lembron areas indicate Late Jurassic to Early Cretaceous ages for the formations that were previously believed to be from the Lower Tertiary period associated with the siderolthic period. Therefore, this study has brought forward or clarified the following points:

[61] 1. In spite of the heterogeneity of the siderolithic paleoweathering facies, stable and coherent paleomagnetic data were obtained. Late silica impregnation of the profile may have enabled the preservation of the paleomagnetic signal.

[62] 2. The new ages obtained in this study have major implications for the geodynamic evolution of the French Massif Central. Our results suggest a lack of sedimentary cover at the Jurassic-Cretaceous boundary. All detrital elements found in these formations are derived from the basement or eventually from the Permo-Carboniferous formations. In thin sections, detrital elements derived from Mesozoic cherts and sandstones have not been identified. This implies that during the deposition of the Lembron red formations the basement was cropping out and devoid of any Mesozoic cover or residual formations derived from the

weathering of such cover. Furthermore, the profiles are not compacted. In particular, illuviation features and clayey cutans do not show any evidence of compaction, which would have occurred if they had been buried under a thick cover.

[63] 3. The development of these paleoweathering profiles probably corresponds to a long-lasting continental evolution and landscape stability. The disposition of the siderolithic paleoprofiles against fault scarps, around inselbergs, and in filling paleovalleys corresponds with contrasted paleolandscapes on the crystalline basement during the Late Jurassic to Early Cretaceous periods. These records allow completion of the landscape mosaic of western Europe comprising basement-contrasted landscapes; they records also provide insight into the formation of bauxite and the development of swamp landscapes [*Thiry et al.*, 2006].

[64] 4. The data obtained in this study increase our knowledge of the Early Cretaceous continental weathering conditions and paleoclimate. The thick kaolinitic paleoweathering profiles are most likely related to bauxite deposits in the North Mediterranean area developing at this period. This corresponds with effective weathering processes during the Late Jurassic to Early Cretaceous periods, which may have been strengthened by the high CO_2 content of the paleoatmosphere [*Schmitt*, 1999]. Moreover, the systematic silica impregnation that follows the kaolinitic alteration indicates a climatic change from rather humid to dry conditions.

[65] **Acknowledgments.** The paleomagnetism analyses were supported by the National Radioactive Waste Management agency (ANDRA, order 033879). This is IPGP contribution 3001. Scientific discussions with Régine Simon-Coinçon (Mines ParisTech), Florence Quesnel, and Hervé Theveniault (BRGM) greatly contributed to improving this manuscript. Thanks to Bernard Henry and Maxime Legoff (IPGP), as well as to Catherine Kissel (LSCE), for their welcome and their scientific help and discussions, and also to Christine Franke (Mines ParisTech) for language editing. The authors thank Stuart Gilder (Associate Editor), as well as Michael Jackson, Mark Hounslow, and Phil Schmidt (reviewers), for adding constructive comments and suggestions that strengthened this paper.

References

Acton, G. D., and W. A. Kettles (1996), Geologic and palaeomagnetic constraints on the formation of weathered profiles near Inverell, Eastern Australia, *Palaeogeogr. Palaeoclimatol. Palaeoecol.*, *126*, 211–225.

Berner, R. A., and Z. Kothavala (2001), GEOCARB III: A revised model of atmospheric CO_2 over Phanerozoic time, *Am. J. Sci.*, *3001*, 182–204.

Besse, J., and V. Courtillot (2002), Apparent and true polar wander and the geometry of the geomagnetic field over the last 200 Myr, *J. Geophys. Res.*, *107*(B11), 2300, doi:10.1029/2000JB000050.

Besse, J., and V. Courtillot (2003), Apparent true polar wander and the geometry of the geomagnetic field over the last 200 Myr: Correction, *J. Geophys. Res.*, *108*(B10), 2469, doi:10.1029/2003JB002684.

Boulanger, M. C. (1844), *Statistique Géologique et Minéralurgique du Département de l'Allier*, 482 pp., P. A. Desrosiers, Moulins, France.

Brewer, R. (1964), *Fabric and Mineral Analysis in Soils*, 470 pp., Wiley, New York.

Cantinolle, P., P. Didier, J. D. Meunier, C. Parron, J. L. Guendon, G. Bocquier, and D. Nahon (1984), Kaolinites ferrifères et oxyhydroxydes de fer et d'alumine dans les bauxites des Canonnettes (S.E. de la France), *Clay Miner. 19*, 125–135.

Cogné, J. P. (2003), PaleoMac: a Macintosh™ application for treating paleomagnetic data and making plate reconstructions, *Geochem. Geophys. Geosyst.*, *4*(1), 1007, doi:10.1029/2001GC000227.

Correns, C. W., and W. Engelhardt (1941), Röntgenographische Untersuschungen über den Mineralbestand sedimentärer Eisenerze, *Nachr. Akad. Wiss. Goettingen*, *213*, 131–137.

de Launay, L. (1892–93), Etude sur le plateau central. I. La Vallée du Cher dans la région de Montluçon, *Bull. Serv. Carte Geol. Fr.*, *30*, 289-328.

Deschamps, M. (1973), Etude géologique du sidérolithique du Nord-Est, du centre du Massif central français et des terrains qui lui sont associés, thesis, 1270 pp., Univ. Paris IV, Paris.

Dormann, J. L., D. Fiorani, and E. Tronc (1997), Magnetic relaxation in fine-particle systems, *Adv. Chem. Phys.*, *98*, 283–494.

Dunlop, D. J., and Ö. Özdemir (1997), *Rock Magnetism: Fundamentals and Frontiers*, 573 pp., Cambridge Univ. Press, Cambridge, U. K.

Eschenbrenner, V. (1986), Contribution des termites à la micro-agrégation des sols tropicaux, *Cah. ORSTOM, Ser. Pedol.*, *22*(4), 397–408.

Eschenbrenner, V. (1988), Les glébules des sols de Côte d'Ivoire: Nature et origine en milieu ferrallitique, modalités de leur concentration, rôle des termites, thesis, Univ. Dijon, Dijon, France

Fisher, R. A. (Ed.) (1953), Dispersion on a sphere, *Philos. Trans. R. Soc. London, Ser. A*, *217*, 295 pp.

Fitzpatrick, R. W., and U. Schwertmann (1982), Al-substituted goethite: An indicator of pedogenetic and other weathering environments in South Africa, *Geoderma*, *27*, 335–347.

Gehring, A. U., P. Keller, and F. Heller (1992), Magnetic evidence for the origin of lateritic duricrusts in southern Mali (western Africa), *Palaeogeogr. Palaeoclimatol. Palaeoecol.*, *95*, 33–40.

Genise, J. F., and T. M. Bown (1994), New trace fossils of termites (Insecta: Isoptera) from the late Eocene-early Miocene of Egypt, and the reconstruction of the ancient isopteran social behavior, *Ichnos*, *3*, 155–183.

Hasiotis, S. T. (2003), Complex ichnofossils of solitary and social soil organisms: Understanding their evolution and roles in terrestrial paleoecosystems, *Palaeogeogr. Palaeoclimatol. Palaeoecol.*, *192*, 259–320.

Idnurm, M., and P. W. Schmidt (1986), Paleomagnetic dating of weathering profiles, *Geol. Surv. India Mem.*, *120*, 79–88.

Kirschvink, J. L. (1980), The least-squares line and plane and the analysis of paleomagnetic data, *Geophys. J. R. Astron. Soc.*, *62*, 699–718.

Maher, B. A. (1986), Characterization of soils by mineral magnetic measurements, *Phys. Earth Planet. Inter.*, *42*, 76–92.

Martin, L. D. (1995), The recognition and use of dermestid (Insecta, Coleoptera) pupation chambers in paleoecology, *Palaeogeogr. Palaeoclimatol. Palaeoecol.*, *113*, 303–310.

Mathé, P. E. (1996), Application du paléomagnétisme et du magnétisme des roches à l'étude des processus d'altération supergène, doctorate thesis, 210 pp., Univ.'Aix-Marseille 3, Aix-Marseille, France.

McFadden, P. L. (1982), Rejection of paleomagnetic observations, *Earth Planet. Sci. Lett.*, *61*(2), 392–395, doi:10.1016/0012-821X(82)90069-3.

McFadden, P. L., and M. W. McElhinny (1988), The combined analysis of remagnetization circles and direct observation in palaeomagnetism, *Earth Planet. Sci. Lett.*, *87*, 161–172.

Muggler, C. C., J. J. Van Loef, P. Buurman, and J. D. J Van Doesburg (2001), Mineralogical and (sub)microscopic aspects of iron oxides in polygenetic Oxysols form Minas Gerais, Brazil, *Geoderma*, *100*(1-2), 147–171.

Mullins, C. E. (1977), Magnetic susceptibility of the soils and its significance in sol science: A review, *J. Soil Sci.*, *28*, 223–246.

Nahon, D., C. Janot, A. M. Karpoff, H. Paquet, and Y. Tardy (1977), Mineralogy, petrology, and structures of iron crusts (ferricretes) developed on sandstones in the western part of Senegal, *Geoderma*, *19*, 263–277.

Néel, M. L. (1949), Théorie du trainage magnétique des ferromagnétiques en grains fins avec applications aux terres cuites, *Ann. Geophys.*, *5*(2), 99–136.

Norrish, K., and R. M. Taylor (1961), The isomorphous replacement of iron by aluminium in soil goethites, *J. Soil Sci.*, *12*(2), 294–306.

Nott, J. F., M. Idnurm, and R. W. Young (1991), Sedimentology, weathering, age, and geomorphological significance of Tertiary sediments on the far coast of New South Wales, *Aust. J. Earth Sci.*, *38*, 357–373.

Rayot, V. (1994), Altérations du centre de l'Australie: Rôle des solutions salines dans la genèse des silcrètes et des profils blanchis, *Mem. Sci. Terre*, *22*, 142 pp., Ecole Natl. Supér. des Mines de Paris, Paris.

Ricordel, C. (2007), Datations par paléomagnétisme des paléoaltérations du Massif central et de ses bordures: Implications géodynamiques, doctorate thesis, 172 pp., Ecole des Mines, Paris.

Schmidt, P. W., and B. J. J. Embleton (1976), Paleomagnetic results from sediments of the Perth Basin, Western Australia, and their bearing on the timing of regional lateritization, *Palaeogeogr. Palaeoclimatol. Palaeoecol.*, *19*, 257–273.

Schmidt, P. W., and C. D. Ollier (1988), Palaeomagnetic dating of late Cretaceous to early Tertiary weathering in New England, N. S. W., Australia, *Earth Sci. Rev.*, *25*, 363–371.

Schmidt, P. W., V. Prasad, and P. K. Ramam (1983), Magnetic ages of some Indian laterites, *Palaeogeogr. Palaeoclimatol. Palaeoecol.*, *44*, 185–202.

Schmitt, J.-M. (1999), Weathering, rainwater and atmosphere chemistry: Example and modeling of granite weathering in present conditions in a

CO_2-rich, and in an anoxic paleoatmosphere, in *Palaeoweathering, Palaeosurfaces and Related Continental Deposits*, vol. 27, edited by M. Thiry and R. Simon-Coinçon, pp. 21–41, Blackwell Sci., Oxford, U. K.

Schwertmann, U. (1988), Goethite and haematite formation in the presence of clay mineral and gibbsite at 25°C, *Soil Sci. Soc. Am. J.*, *52*, 288–291.

Tauxe, L., T. A. T Mullender, and T. Pick (1996), Potbellies, wasp-waists, and superparamagnetism in magnetic hysteresis. *J. Geophys. Res.*, *101*, 571–583.

Théveniaut, H., and P. Freyssinet (1999), Paleomagnetism applied to lateritic profiles to assess saprolite and duricrust formation processes: The example of the Mont Baduel profile (French Guiana), *Palaeogeogr. Palaeoclimatol. Palaeoecol.*, *148*, 209–231.

Théveniaut, H., F. Quesnel, R. Wyns, and G. Hugues (2007), Paleomagnetic dating of the "Borne de Fer" ferricrete (NE France): Lower Cretaceous continental weathering, *Palaeogeogr. Palaeoclimatol. Palaeoecol.*, *253*, 271–279.

Thiry, M., and A. R. Milnes (1989), Pedogenic and groundwater silcretes at Stuart Creek Opal Field, South Australia, *J. Sediment. Petrol.*, *61*(1), 111–127.

Thiry, M., and M. Turland (1985), Paléoséquences de sols ferrugineux et de cuirassements siliceux dans le Sidérolitique du Nord du Massif central (bassin de Montluçon-Domérat), *Geol. Fr.*, *2*, 175–192.

Thiry, M., et al. (2006), Continental France and Belgium during the Early Cretaceous: Paleoweatherings and paleolandforms, *Bull. Soc. Geol. Fr.*, *177*(3), 155–175.

Thiry, M., J. M. Schmitt, N. Trauth, R. Cojean, and M. Turland (1983), Formations rouges "sidérolithiques" et silicifications sur la bordure Nord du Massif central, *Rev. Geol. Phys. Geol. Dyn.*, *24*, 381–395.

Wielemaker, W. G. (1984), Soil formation by termites a study in the Kisii area, Kenya, doctorate thesis, 132 pp., *Dep. of Soil Sci. and Geol., Agric. Univ.*, Wageningen, Netherlands.

Yans, J. (2003), Chronologie des sédiments kaoliniques faciès wealdiens (Barrémien moyen Albien supérieur; Bassin de Mons) et de la saprolite polyphasée (Crétacé inférieur et Miocène inférieur) de la Haute-Lesse (Belgique). Implications géodynamiques et paléoclimatiques, doctorate thesis, 316 pp., *Fac. Polytech. de Mons*, Univ. de Paris-Sud Orsay, Paris.

Zijderveld, J. D. A. (1967), A. C. demagnetization of rocks: Analysis of results, in *Methods in Paleomagnetism*, edited by D. W. Collinson, K. M. Creer, and S. K. Runcorn, pp. 254–286, Elsevier, Amsterdam.

F. Lagroix and M.-G. Moreau, Institut de Physique du Globe de Paris, 4, place Jussieu-Case 89, F-75252 Paris CEDEX 05, France.

C. Ricordel-Prognon, BRGM GEO/G2R, 3 av. Claude Guillemin, BP 60009, F-45060 Orleans CEDEX, France. (c.prognon@brgm.fr)

M. Thiry, Mines ParisTech, 35 rue Saint Honoré, F-77305 Fontainebleau, France.